

Diffracting molecular matter-waves at deep-ultraviolet standing-light waves

Ksenija Simonović,^{1,*} Richard Ferstl,¹ Alfredo Di Silvestro,² Marcel Mayor,² Lukas Martinetz,³ Klaus Hornberger,³ Benjamin A. Stickler,⁴ Christian Brand,⁵ and Markus Arndt^{1,†}

¹University of Vienna, Faculty of Physics, VDS, VCQ, Boltzmannngasse 5, A-1090 Vienna, Austria

²Department of Chemistry, University of Basel, St. Johannisring 19, 4056 Basel, Switzerland

³University of Duisburg-Essen, Lotharstraße 1, 47048 Duisburg, Germany

⁴Ulm University, Institute for Complex Quantum Systems and Center for Integrated Quantum Science and Technology, Albert-Einstein-Allee 11, 89069 Ulm, Germany

⁵German Aerospace Center (DLR), Institute of Quantum Technologies, Wilhelm-Runge-Straße 10, 89081 Ulm, Germany

(Dated: August 2, 2024)

Matter-wave interferometry with molecules is intriguing both because it demonstrates a fundamental quantum phenomenon and because it opens avenues to quantum-enhanced measurements in physical chemistry. One great challenge in such experiments is to establish matter-wave beam splitting mechanisms that are efficient and applicable to a wide range of particles. In the past, continuous standing light waves in the visible spectral range were used predominantly as phase gratings, while pulsed vacuum ultraviolet light found applications in photo-ionisation gratings. Here, we explore the regime of continuous, intense deep-ultraviolet (>1 MW/cm², 266 nm) light masks, where a rich variety of photo-physical and photo-chemical phenomena and relaxation pathways must be considered. The improved understanding of the mechanisms in this interaction opens new potential pathways to protein interferometry and to matter-wave enhanced sensing of molecular properties.

INTRODUCTION

Shortly after Louis de Broglie’s prediction that one needs to ‘associate a periodical phenomenon with any isolated portion of matter or energy’ and that we should see this ‘in phase with a wave’ [1], matter-waves were experimentally confirmed for electrons [2, 3], neutral He atoms and H₂ molecules [4], as well as for neutrons [5]. De Broglie’s revolutionary proposal about the wave behaviour of matter [1] started the theoretical formulation of modern quantum physics [6] and quantum chemistry, where this idea is at the heart of molecular bond and orbital theory [7, 8]. While in chemistry electron quantum waves are usually confined inside an atom or molecule, a whole research field has evolved around the question how to describe the center-of-mass motion of single and composite systems – from electrons [9] over neutrons [10] and atoms [11, 12] to complex molecules [13] or even antimatter [14].

Here, we are focusing on new tools for the quantum coherent manipulation of the centre-of-mass motion of large molecules, inspired by advances in atom interferometry and progress in the diffraction of cold dimers [15], small noble gas clusters [16, 17], and large molecules [18]. Numerous molecule interferometers have been built throughout the last two decades to explore molecular transition strengths [19, 20], to study the quantum wave nature of fullerenes [21], vitamins [22], polypeptides [23], clusters of organic molecules [24] or tailor-made compounds with masses even beyond 25 kDa [25]. A variety of recent experiments in physical chemistry have focused on the analysis of molecules and clusters in classical and quantum beam deflectometry [26–31]. These studies find a valuable complement in matter-wave interferometry which also allows measuring the electric [32], magnetic [33], optical [34] or structural properties [32, 35, 36] of complex molecules via deflection of fine-grained quantum interference fringes.

Extending matter-wave interferometry to an even larger

set of molecules requires new methods for molecular beam generation, beam splitters, and efficient single-molecule detectors. Here, we focus on how to realise deep ultraviolet beam splitters and how they interact with the rich set of internal molecular properties. Inspired by early achievements in atom optics [37, 38], nanomechanical masks were already successfully used to manipulate molecular beams [18, 39–41]. While these nanostructures are very well suited for many atoms and molecules with low electric polarisability and dipole moments [42, 43], optical gratings cannot be clogged or destroyed. They are perfectly periodic, adjustable in situ and in real time and they may also exploit internal states that nanomasks would not be sensitive to.

Inspired by prior experiments in atom optics [44–46] and electron optics [47], optical phase gratings were realised for molecular beams of fullerenes [48] and even antibiotics [49] and pulsed vacuum-ultraviolet photo-ionisation gratings as matter-wave beam splitters for organic clusters [24] and polypeptides [23]. Here, we study the regime of continuous, high-intensity deep-ultraviolet (DUV) light masks. The wavelength of $\lambda_L = 266$ nm is close to a (very broad) electronic transition in many aromatic molecules and high-power laser light can be generated with high coherence and in a good beam profile by second harmonic generation of a diode pumped solid state laser. For thermal beams of molecules with an absorption cross-section around $\sigma_{\text{abs}} \simeq 10^{-16}$ cm² and velocities in the range of 100–300 m/s, laser intensities around 1 MW/cm² are required to ensure that selected chromophores absorb one or a few photons during their transit through the laser beam. Here, we demonstrate the realization of such optical gratings and discuss how the internal state evolution after the absorption process influences the evolution of the quantum wave that is associated with the molecular center-of-mass motion.

We specifically compare the four molecules shown in Fig. 1(a): *meso*-tetraphenylporphyrin (TPP, $m = 614.7$ u),

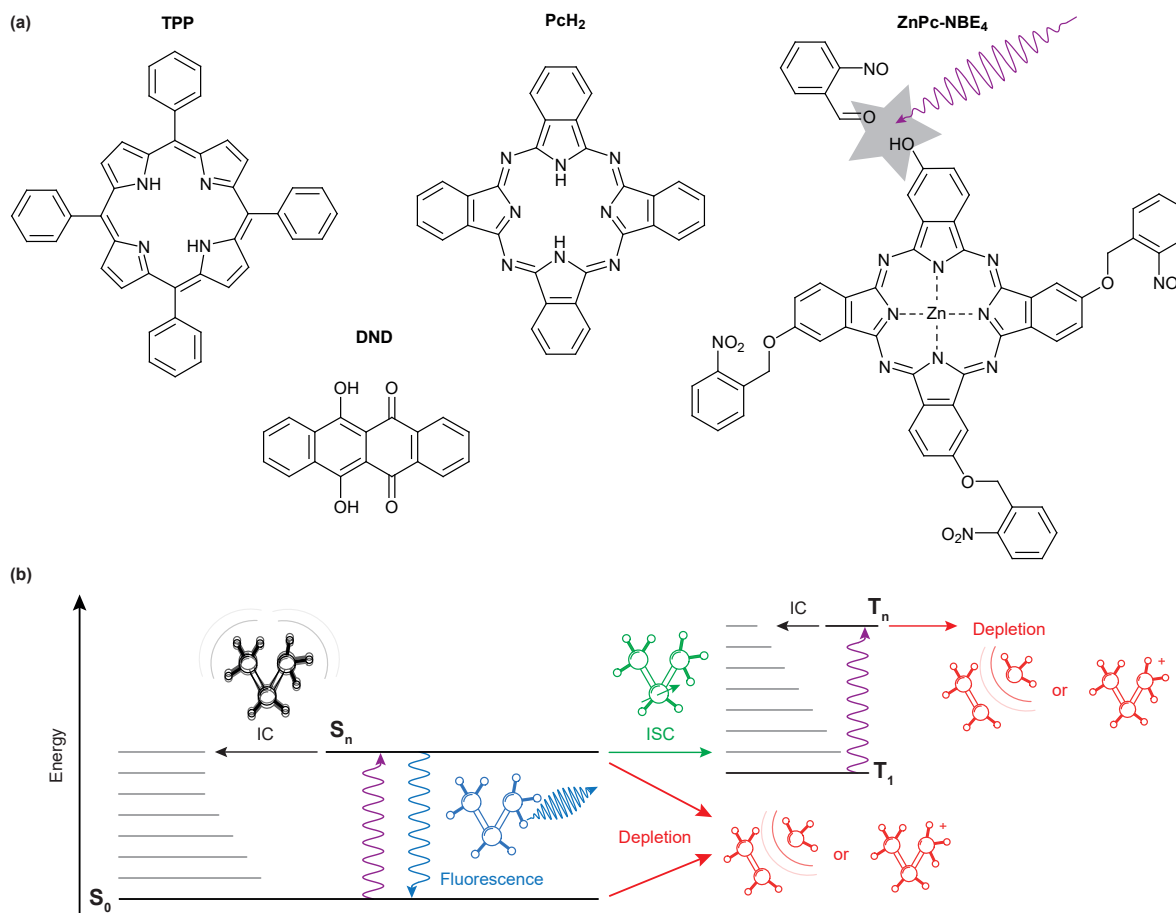


FIG. 1. (a): Molecules explored in this experiment, from left to right: *meso*-Tetraphenylporphyrin (TPP), 6,11-Dihydroxy-5,12-naphthacenedione (DND), metal-free phthalocyanine (PcH₂), a zinc-coordinated phthalocyanine derivative (ZnPc-NBE₄). (b): Possible internal relaxation pathways after deep-ultraviolet photo-excitation. After electronic excitation, the emission of a fluorescence photon adds a randomly oriented photon recoil to the molecule, blurring the respective diffraction peaks. This is not the case for non-radiative processes, such as internal conversion and inter-system crossing. Fragmentation or ionisation may occur from any excited state or a hot ground state molecule, removing it effectively from the beam.

6,11-dihydroxy-5,12-naphthacenedione (DND, and $m = 290.3$ u), phthalocyanine (PcH₂, $m = 514.5$ u) and a zinc-coordinated phthalocyanine where each isoindole unit is bound to an *ortho*-nitro benzylic ether (NBE) group as a photocleavable tag (ZnPc-NBE₄, $m = 1182.4$ u). TPP, DND, and PcH₂ were obtained commercially (Sigma Aldrich/Merck) and used without further purification while ZnPc-NBE₄ was synthesized by us based on a phthalocyanine core (see ESI). We use these different systems to explore the role of different molecular energy relaxation pathways some of which are indicated in the level scheme of Fig. 1(b). They include internal conversion (IC), intersystem crossing (ISC), fluorescence, and the bond dissociation of a photocleavable tag. We discuss how these internal effects influence the de Broglie wave, i.e. the quantum evolution of the molecular center-of-mass motion, and how to observe it in experiments.

EXPERIMENTAL SETUP

The idea of the experiment is shown in Fig. 2. All molecules are sublimated in a thermal source and the resulting beam is collimated to an angle below $5 \mu\text{rad}$. Molecules of different velocity are spatially dispersed by their free-flight parabolas with a $20 \mu\text{m}$ high delimiter immediately behind the grating (not shown). This slit additionally ensures that all detected molecules have interacted with the light grating. The molecules propagate another 0.7 m until they hit a thin quartz slide at the end of the vacuum chamber, where they are imaged using laser-induced fluorescence microscopy [50], see ESI for details.

To realise the standing wave laser grating, 5 W of laser radiation at $\lambda_L = 532$ nm is frequency doubled in an external resonator (Sirah Wavetrain) to $\lambda_L = 266$ nm with an output power of about 1.2 W. The DUV light is focused onto a dielectric mirror in high vacuum, with its surface aligned parallel to the molecular beam. To protect the laser from back-reflected light, and also to control the grating power, we

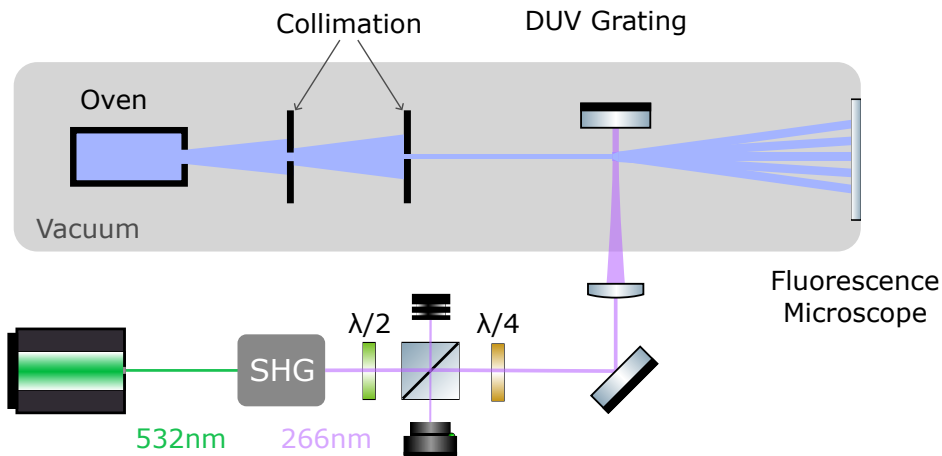


FIG. 2. Setup of the experiment: A thermal molecular beam is collimated to a divergence of $5\ \mu\text{rad}$ to approximate a plane-parallel matter-wave. The molecules are diffracted at a deep ultraviolet grating which is generated as a standing light wave of a high-power continuous frequency doubled laser. The diffracted molecules generate a mass density pattern on the window of that vacuum chamber, which is imaged using fluorescence microscopy. During diffraction, the matter-wave beam splitter imparts a transverse momentum of $\Delta p = \pm n\hbar k_L$, with the integer n depending on the details of the process.

employ an optical isolator, consisting of a $\lambda/2$ plate in front of a polarising beam splitter and a $\lambda/4$ plate behind it. The light in the optical grating is therefore circularly polarized. We track the power of the retro-reflected DUV beam and find that it is stable to within 10% during a measurement. However, irradiating the mirror with light intensities beyond $1\ \text{MW}/\text{cm}^2$ at 10^{-7} mbar leads to a slow degradation of the mirror surface. To compensate for this, we shift the mirror parallel to the molecular beam in between measurements to expose a fresh spot to the laser. Given a grating period of $\lambda_L/2 = 133\ \text{nm}$ and a laser waist of $12 - 15\ \mu\text{m}$ [51], the molecular beam divergence and its inclination to the mirror surface have to be smaller than 1 mrad, to ensure that all molecules see a well-defined optical grating.

While many aspects of matter-wave diffraction can be surprisingly well described using undergraduate level mathematics of waves [52], accounting for all experimental details and molecular processes requires a full quantum description. Our model accounts for the interaction between the molecules and the optical grating, the role of finite coherence and decoherence, the source collimation and velocity distribution and many internal relaxation pathways. The complete theory is based on propagating Wigner functions, as described in a separate paper [53] and summarised in the ESI. Here, we focus on the conceptual discussion of the relevant processes.

As long as photon absorption can be neglected, the standing light wave acts as a pure phase grating: The interaction between the oscillating laser field and the dynamical polarisability α_{266} of the molecule imposes a periodic dipole potential onto the molecular centre-of-mass motion, which modulates the phase of the molecular matter-wave along the x -axis:

$$\Delta\phi(x) \propto \frac{\alpha_{266}P_L}{\varepsilon_0 c w_y v_z} \cos^2\left(\frac{2\pi x}{\lambda_L}\right). \quad (1)$$

Here, P_L is the laser power, w_y the vertical waist of the Gaus-

sian laser beam, v_z the forward molecular velocity, and c the speed of light. The phase modulation results in a discrete momentum transfer to the molecule in even multiples of the photon momentum $\Delta p = \pm 2n\hbar k_L$, where $n \in \mathbb{N}$ and the photon wave number is $k_L = 2\pi/\lambda_L$. This phase modulation of the matter-wave translates into a discrete spatial distribution of the molecular arrival probability density on the detector further downstream. This interaction is always present, since every molecule has a finite and sometimes even a large dynamical polarizability.

The description is more involved when the molecule can also absorb at least one photon from the laser grating. In this case, it receives an additional recoil of $\pm\hbar k_L$ per photon. This gives rise to additional peaks exactly half way in between the diffraction orders associated with the phase grating. Even though the absorption process is probabilistic and follows a Poisson distribution, it is coherent in the sense that one cannot, not even in principle, distinguish if the photon was absorbed while it was on the way towards the mirror or back. This is due to the long coherence length (here 50 m) of our DUV laser light [54, 55]. At high intensities, absorption of N photons can thus disperse the molecular momentum in integer multiples of the photon momentum, $\Delta p = n\hbar k_L$ with $n = -N, \dots, N$, and all branches of the molecular distribution associated with an even number of photons overlap at the detector position-synchronously with those affected by the phase grating alone, even though their internal state is different.

If an excited molecule decays non-radiatively, for instance by internal conversion (IC) or inter-system crossing (ICS) to a triplet state, the momentum transfer to the molecule is determined by the phase and absorption component alone. However, if spontaneous fluorescence is emitted near the grating, this adds again a momentum kick. Since the direction of spontaneously emitted photons is isotropically distributed, fluorescence would show up as a broadening of the diffrac-

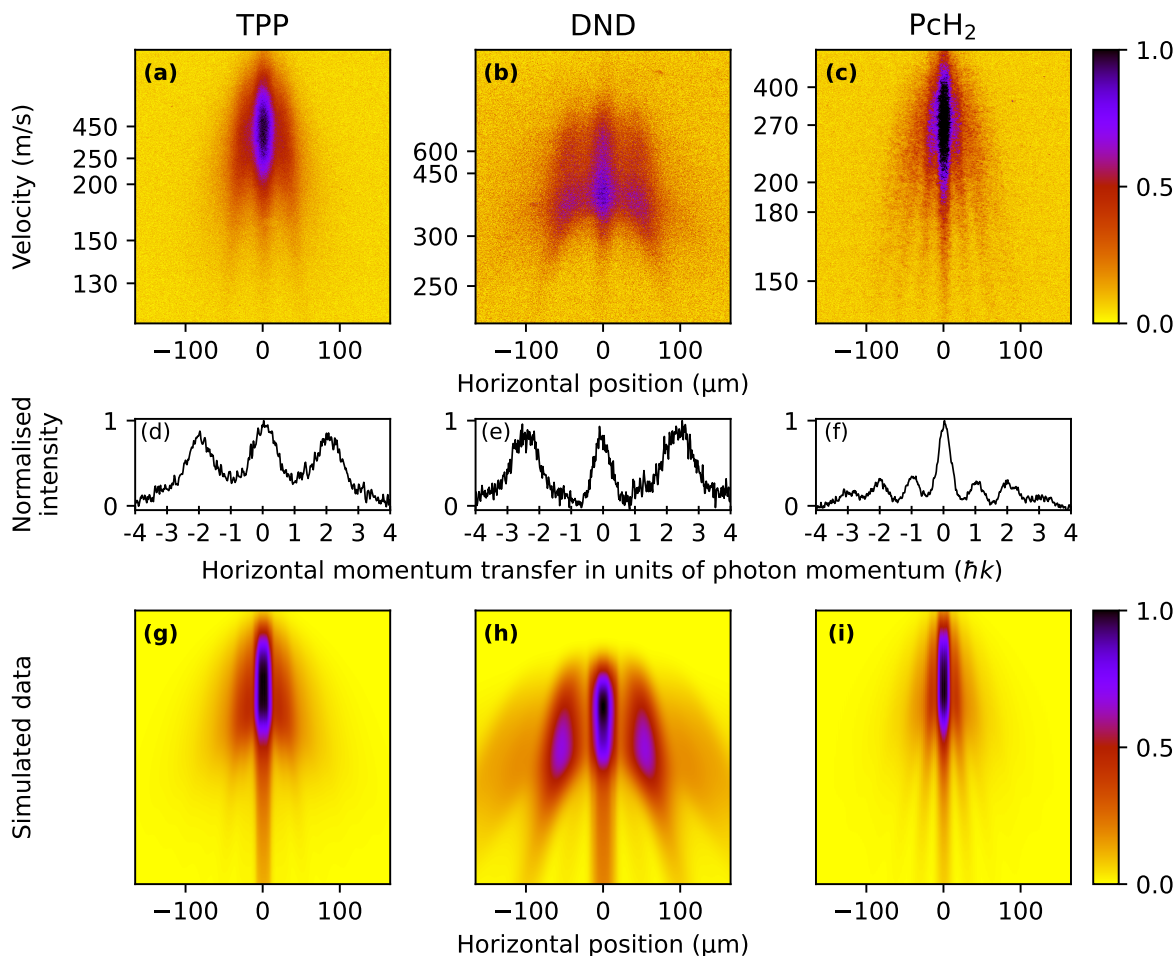


FIG. 3. **Top row:** Fluorescence micrographs of the molecular interferograms: While the phase grating character dominates for TPP (a), photon absorption gains importance for phthalocyanine (c). **Middle row:** Normalised traces for each of the fluorescence micrographs above, rescaled to the same momentum transfer and integrated over the lower two thirds of each image. **Bottom row:** The numerical simulation shows good agreement with the experiment and allows corroborating the molecular ultraviolet polarizability and absorption cross section.

tion peaks. Even multiple absorption-relaxation cycles are conceivable, given the range of absorption cross-sections and the laser intensities in our experiment.

Finally, the energy of a single or several photons may suffice to cleave the molecule. Our design and synthesis of ZnPc-NBE₄ was based on the idea that molecules should be selectively removed from the molecular beam upon photo-cleavage in the antinodes of the light grating and the fragments would be kicked to beyond the acceptance angle of the fluorescence detector (0.5 mrad).

RESULTS AND DISCUSSION

We start our discussion with the diffraction pattern of TPP, as shown in Fig. 3(a). It encompasses molecular velocities from 130 to beyond 450 m s⁻¹ which are dispersed on the detector because of their free fall in the gravitational field. Based on our knowledge of the de Broglie wavelength $\lambda_{dB} = h/(mv) \approx 4 - 5$ pm for the slower molecules and the grating

period $d = \lambda_L/2$, we can attribute diffraction to the effect of a dipole phase grating ($\Delta p = n2\hbar k$), with only little background. To search for an effect of photo absorption and emission we show the results for DND in Fig. 3(b). The wider separation of the fringes is due to its smaller molecular weight and larger de Broglie wavelength. And here, we observe well-defined peaks half-way in between the diffraction orders associated with the phase grating. As all peaks have about the same width we see no indication for molecular fluorescence near the grating.

In solution, phthalocyanine is measured to have a good absorption cross section of $\sigma_{266} = 1.1 \times 10^{-16}$ cm². We show its diffraction pattern in Fig. 3(c). Indeed, single-photon recoil shows up as clearly discernible peaks of the transverse momentum, at multiples of the photon momentum $\pm 1\hbar k_L$. Again, the diffraction fringes are all equal, indicating that fluorescence plays no major role. Because of their absorption properties, phthalocyanine derivatives are interesting candidates for photo-cleavage studies, when we decorate the core unit with four photo-reactive ortho-nitro benzaldehyde

group (NBE). Their photon absorption cross section in solution is even about a factor of two higher than that of the phthalocyanine core alone. Earlier studies have already shown that a photo-reaction can release an ortho-nitroso benzaldehyde selectively even from a protein in the gas phase [56]. Our matter-wave diffraction experiments with this molecule yield a diffraction image that resembles the result of unlabelled phthalocyanine. This invites two complementary interpretations which are discussed in detail in the ESI. The similarity of the PcH_2 and ZnPc-NBE_4 diffraction images can be explained within the frame work of matter-wave diffraction by the magnitude of the molecular de Broglie wavelengths and the expected photodepletion process. Another option is that the molecule may thermally decompose entirely in the source already. We find that here the thermal fragmentation precedes the optical dissociation, which demonstrates the high sensitivity of the NBE groups to the addition of internal energy. Since similar molecules are known to survive ultrafast laser evaporation in particular when injected into a cooling carrier gas or electrospray ionisation, photo-cleavage is still a promising basis for a deep ultraviolet beam splitter. The relevant effects and the theory apply as described above. This insight opens a path to future explorations of peptide and protein interferometry.

CONCLUSION

We have shown that a deep ultra-violet standing light wave can act as a versatile beam splitter for organic molecules. This opens the door to the manipulation of novel particles and also to acquiring new information on photo-physical processes in molecules in the gas phase. Compared to typical spectroscopy methods the deactivation process is not encoded in the population of a final state but in the molecular center-of-mass motion, i.e. the spatial diffraction pattern, where we can detect each molecule in principle with single molecules sensitivity [50]. While the signal-to-noise in our present setup is still too low for precision measurements, better sources will validate the concept in the future. The rich set of internal states of molecules will also allow us to explore a variety of additional photo-physical and photo-chemical effects for beam splitting and molecular analysis: For instance, when molecules are optically excited to long-lived triplet states, beam deflection in a magnetic field can be sensitively read out from interference patterns. Similarly, photo-isomerisation in the DUV grating will serve as a measurement-induced beam splitter when the detector at the end is sensitive and specific with regard to the molecular conformers. We envisage that intense deep UV light gratings will become important building blocks for many all-optical matter-wave interferometers, designed to explore molecular quantum optics in the regime of high mass and high complexity.

AUTHOR CONTRIBUTIONS

Conceptualisation: MA, CB, KS, RF, MM.
 Formal Analysis: LM, BS, KH, RF.
 Materials and synthesis: ADS, MM.
 Funding acquisition: MA, KH, MM.
 Investigation: KS, RF, LM, CB.
 Methodology: all authors.
 Software: LM, RF.
 Supervision: MA, CB, KH, BS, MM.
 Writing – original draft: MA, CB, KS, RF.

CONFLICTS OF INTEREST

There are no conflicts to declare.

DATA AVAILABILITY

Data for this article and ESI, including raw, background-corrected and preprocessed diffraction images, as well as data files for simulated images, are available at zenodo repository under <https://doi.org/10.5281/zenodo.13124328>.

ACKNOWLEDGEMENTS

We thank Y. Hua and V. Köhler for measuring the solution spectra of the photocleavable molecules and we thank D. Vörös, L. González and A. Shayeghi for fruitful discussions. This research was funded in whole, or in part, by the Austrian Science Fund (FWF) [10.55776/DOC85] and [10.55776/P32543]. We acknowledge funding by the European Commission within project 860713, by the Gordon & Betty Moore Foundation within project 10771, and by the German Aerospace Center (DLR) within project 50WM2264, with funds provided by the German Federal Ministry for Economic Affairs and Climate Action (BMWK). BAS acknowledges funding by the DFG–510794108 as well as by the Carl-Zeiss-Foundation through the project QPhoton.

* ksenija.simonovic@univie.ac.at

† markus.arndt@univie.ac.at

- [1] L. De Broglie, *Nature*, 1923, **112**, 540–540.
- [2] C. Davisson and L. H. Germer, *Physical Review*, 1927, **30**, 705–740.
- [3] G. P. Thomson, *Nature*, 1927, **120**, 802–802.
- [4] I. Estermann and O. Stern, *Zeitschrift für Physik*, 1930, **61**, 95–125.
- [5] H. v. Halban Jnr. and P. Preiswerk, *C.R. Acad. Sci. Paris*, 1936, **203**, 73–75.
- [6] E. Schrödinger, *Physical Review*, 1926, **28**, 1049–1070.
- [7] R. S. Mulliken, *Physical Review*, 1928, **32**, 186–222.
- [8] L. Pauling, *Journal of the American Chemical Society*, 1931, **53**, 1367–1400.

- [9] F. Hasselbach, *Reports on Progress in Physics*, 2009, **73**, 016101.
- [10] H. Rauch and S. A. Werner, *Neutron Interferometry*, Oxford University Press, 2nd edn, 2015.
- [11] A. D. Cronin, J. Schmiedmayer and D. E. Pritchard, *Reviews of Modern Physics*, 2009, **81**, 1051–1129.
- [12] G. M. Tino and M. A. Kasevich, *Atom Interferometry*, IOS Press, Amsterdam, Netherlands, 2014.
- [13] K. Hornberger, S. Gerlich, P. Haslinger, S. Nimmrichter and M. Arndt, *Reviews of Modern Physics*, 2012, **84**, 157–173.
- [14] S. Sala, A. Ariga, A. Ereditato, R. Ferragut, M. Giammarchi, M. Leone, C. Pistillo and P. Scamporrì, *Science Advances*, 2019, **5**, eaav7610.
- [15] M. S. Chapman, C. R. Ekstrom, T. D. Hammond, R. A. Rubenstein, J. Schmiedmayer, S. Wehinger and D. E. Pritchard, *Physical Review Letters*, 1995, **74**, 4783–4786.
- [16] W. Schöllkopf and J. P. Toennies, *Science*, 1994, **266**, 1345–1348.
- [17] B. S. Zhao, W. Zhang and W. Schoellkopf, *Molecular Physics*, 2013, **111**, 1772–1780.
- [18] M. Arndt, O. Nairz, J. Vos-Andreae, C. Keller, G. van der Zouw and A. Zeilinger, *Nature*, 1999, **401**, 680–682.
- [19] C. Lisdat, M. Frank, H. Knöckel, M.-L. Almazor and E. Tiemann, *The European Physical Journal D - Atomic, Molecular, Optical and Plasma Physics*, 2000, **12**, 235–240.
- [20] S. Liu, I. Sherstov, C. Lisdat, H. Knöckel and E. Tiemann, *The European Physical Journal D*, 2010, **58**, 369–377.
- [21] B. Brezger, L. Hacker Müller, S. Uttenthaler, J. Petschinka, M. Arndt and A. Zeilinger, *Physical Review Letters*, 2002, **88**, 100404.
- [22] L. Mairhofer, S. Eibenberger, J. P. Cotter, M. Romirer, A. Shayeghi and M. Arndt, *Angewandte Chemie International Edition*, 2017, **56**, 10947–10951.
- [23] A. Shayeghi, P. Rieser, G. Richter, U. Sezer, J. H. Rodewald, P. Geyer, T. J. Martinez and M. Arndt, *Nature Communications*, 2020, **11**, 1447.
- [24] P. Haslinger, N. Dörre, P. Geyer, J. Rodewald, S. Nimmrichter and M. Arndt, *Nature Physics*, 2013, **9**, 144–148.
- [25] Y. Y. Fein, P. Geyer, P. Zwick, F. Kiařka, S. Pedalino, M. Mayor, S. Gerlich and M. Arndt, *Nature Physics*, 2019, **15**, 1242–1245.
- [26] P. Dugourd, I. Compagnon, F. Lepine, R. Antoine, D. Rayane and M. Broyer, *Chemical Physics Letters*, 2001, **336**, 511–517.
- [27] I. Compagnon, F. C. Hagemeister, R. Antoine, D. Rayane, M. Broyer, P. Dugourd, R. R. Hudgins and M. F. Jarrold, *Journal of the American Chemical Society*, 2001, **123**, 8440–8441.
- [28] R. Antoine, I. Compagnon, D. Rayane, M. Broyer, P. Dugourd, G. Breaux, F. C. Hagemeister, D. Pippen, R. R. Hudgins and M. F. Jarrold, *Journal of the American Chemical Society*, 2002, **124**, 6737–6741.
- [29] A. Shayeghi, R. L. Johnston, D. M. Rayner, R. Schäfer and A. Fielicke, *Angewandte Chemie International Edition*, 2015, **54**, 10675–10680.
- [30] T. M. Fuchs and R. Schäfer, *Physical Chemistry Chemical Physics*, 2021, **23**, 11334–11344.
- [31] F. Rivic, T. M. Fuchs and R. Schäfer, *Physical Chemistry Chemical Physics*, 2021, **23**, 9971–9979.
- [32] M. Gring, S. Gerlich, S. Eibenberger, S. Nimmrichter, T. Berrada, M. Arndt, H. Ulbricht, K. Hornberger, M. Müri, M. Mayor, M. Böckmann and N. L. Doltsinis, *Physical Review A*, 2010, **81**, 031604.
- [33] Y. Y. Fein, S. Pedalino, A. Shayeghi, F. Kiařka, S. Gerlich and M. Arndt, *Physical Review Letters*, 2022, **129**, 123001.
- [34] S. Eibenberger, X. Cheng, J. P. Cotter and M. Arndt, *Physical Review Letters*, 2014, **112**, 250402.
- [35] S. Gerlich, M. Gring, H. Ulbricht, K. Hornberger, J. Tüxen, M. Mayor and M. Arndt, *Angewandte Chemie International Edition*, 2008, **47**, 6195–6198.
- [36] J. Tüxen, S. Gerlich, S. Eibenberger, M. Arndt and M. Mayor, *Chemical Communications*, 2010, **46**, 4145–4147.
- [37] D. W. Keith, M. L. Schattenburg, H. I. Smith and D. E. Pritchard, *Physical Review Letters*, 1988, **61**, 1580–1583.
- [38] O. Carnal and J. Mlynek, *Physical Review Letters*, 1991, **66**, 2689–2692.
- [39] T. Reisinger, A. A. Patel, H. Reingruber, K. Fladischer, W. E. Ernst, G. Bracco, H. I. Smith and B. Holst, *Physical Review A*, 2009, **79**, 053823.
- [40] C. Brand, M. Sclafani, C. Knobloch, Y. Lilach, T. Juffmann, J. Kotakoski, C. Mangler, A. Winter, A. Turchanin, J. Meyer, O. Cheshnovsky and M. Arndt, *Nature Nanotechnology*, 2015, **10**, 845–848.
- [41] A. Luski, Y. Segev, R. David, O. Bitton, H. Nadler, A. R. Barnea, A. Goriach, O. Cheshnovsky, I. Kaminer and E. Narevicius, *Science*, 2021, **373**, 1105–1109.
- [42] C. Knobloch, B. A. Stickler, C. Brand, M. Sclafani, Y. Lilach, T. Juffmann, O. Cheshnovsky, K. Hornberger and M. Arndt, *Fortschritte der Physik*, 2017, **65**, 1600025.
- [43] K. Simonović, R. Ferstl, A. Barlow, A. Shayeghi, C. Brand and M. Arndt, *Physical Review Research*, 2024, **6**, 033109.
- [44] P. E. Moskowitz, P. L. Gould, S. R. Atlas and D. E. Pritchard, *Physical Review Letters*, 1983, **51**, 370–373.
- [45] P. L. Gould, G. A. Ruff and D. E. Pritchard, *Physical Review Letters*, 1986, **56**, 827–830.
- [46] E. M. Rasel, M. K. Oberthaler, H. Batelaan, J. Schmiedmayer and A. Zeilinger, *Physical Review Letters*, 1995, **75**, 2633–2637.
- [47] D. L. Freimund, K. Aflatooni and H. Batelaan, *Nature*, 2001, **413**, 142–143.
- [48] O. Nairz, B. Brezger, M. Arndt and A. Zeilinger, *Physical Review Letters*, 2001, **87**, 160401.
- [49] C. Brand, F. Kiařka, S. Troyer, C. Knobloch, K. Simonović, B. A. Stickler, K. Hornberger and M. Arndt, *Physical Review Letters*, 2020, **125**, 033604.
- [50] T. Juffmann, A. Milic, M. Müllneritsch, P. Asenbaum, A. Tsukernik, J. Tüxen, M. Mayor, O. Cheshnovsky and M. Arndt, *Nature Nanotechnology*, 2012, **7**, 297–300.
- [51] C. Brand, K. Simonović, F. Kiařka, S. Troyer, P. Geyer and M. Arndt, *Optics Express*, 2020, **28**, 6164.
- [52] C. Brand, S. Troyer, C. Knobloch, O. Cheshnovsky and M. Arndt, *American Journal of Physics*, 2021, **89**, 1132–1138.
- [53] L. Martinetz, B. A. Stickler, K. Simonović, R. Ferstl, C. Brand, M. Arndt and K. Hornberger, *Probing molecular photophysics in a matter-wave interferometer*, 2024, <https://arxiv.org/abs/2407.18775v1>.
- [54] J. Tomkovič, M. Schreiber, J. Welte, M. Kiffner, J. Schmiedmayer and M. K. Oberthaler, *Nature Physics*, 2011, **7**, 379–382.
- [55] J. P. Cotter, S. Eibenberger, L. Mairhofer, X. Cheng, P. Asenbaum, M. Arndt, K. Walter, S. Nimmrichter and K. Hornberger, *Nature Communications*, 2015, **6**, 7336.
- [56] J. Schätti, M. Krieglleder, M. Debiossac, M. Kerschbaum, P. Geyer, M. Mayor, M. Arndt and V. Köhler, *Chemical Communications*, 2019, **55**, 12507–12510.

Supplementary Information for Diffracting molecular matter-waves at deep-ultraviolet standing-light waves

Ksenija Simonović,^{1,*} Richard Ferstl,¹ Alfredo Di Silvestro,² Marcel Mayor,² Lukas Martinetz,³ Klaus Hornberger,³ Benjamin A. Stickler,⁴ Christian Brand,⁵ and Markus Arndt^{1,†}

¹University of Vienna, Faculty of Physics, VDS, VCQ, Boltzmannngasse 5, A-1090 Vienna, Austria

²Department of Chemistry, University of Basel, St. Johannisring 19, 4056 Basel, Switzerland

³University of Duisburg-Essen, Lotharstraße 1, 47048 Duisburg, Germany

⁴Ulm University, Institute for Complex Quantum Systems and Center for Integrated Quantum Science and Technology, Albert-Einstein-Allee 11, 89069 Ulm, Germany

⁵German Aerospace Center (DLR), Institute of Quantum Technologies, Wilhelm-Runge-Straße 10, 89081 Ulm, Germany
(Dated: August 2, 2024)

IMAGING OF THE DIFFRACTION PATTERNS

The interference patterns are collected on a quartz slide and illuminated by a homogeneous diffuse laser beam. The laser wavelength is chosen to match an excitation resonance of the molecules. TPP is excited by 421 nm light, DND by 266 nm light, and PcH₂ as well as ZnPc–NBE₄ by 661 nm laser light. The fluorescence band pass filters are chosen to match the molecular spectra: 630–670 nm for TPP, 506–594 nm for DND, 698.5–723.5 nm for PcH₂ and 672–712 nm for ZnPc–NBE₄. All fluorescence images were collected for 5 minutes, taking care to eliminate ambient light. We see no evidence of laser-induced fluorescence bleaching during this time except for DND. Even in that case, a 5-minute exposition allows to image with good signal-to-noise. The fluorescence is collected using a 20× Zeiss plan neofluoar objective and imaged by a tube lens ($f = 164$ mm) onto an Andor iXON 3 EMCCD camera, cooled to -75 °C.

DATA PROCESSING

To correct the background signal in our raw images a dark CCD image (no laser) is subtracted by default in the recording software. Additionally we also subtract bright images taken before and after the molecules are deposited. This allows to reduce the contribution of stray light as well as contaminations from dust particles. Regions where obvious strong contaminations cannot be eliminated this way were manually removed from the dataset. We also eliminate intensity spikes by removing the lowest and highest 10^{-5} -quantile of the data. Because of small variations in the ambient light the background subtraction process can still leave inhomogeneities in the image background. They are reduced by subtracting a linear fit to the image that is gained from outside the region of the diffraction pattern. Finally a small rotation of the camera is corrected by rotating the images by 0.4° and the data is cropped to the region of interest where the diffraction pattern is located.

SIMULATIONS

Overview

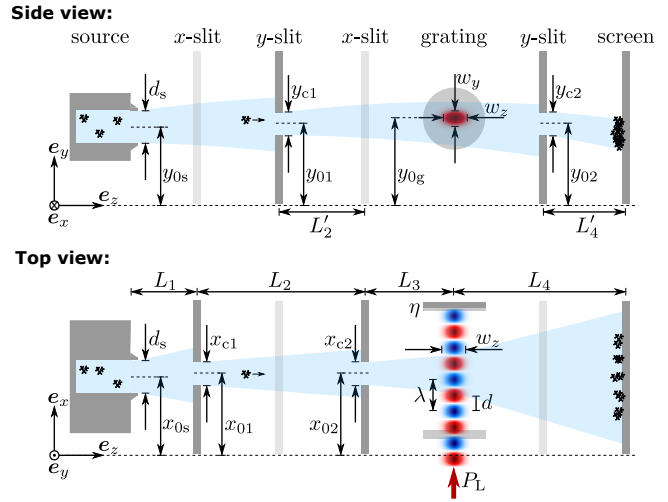


FIG. 1. Schematic depiction of the experimental setup with all simulation-relevant parameters as listed in Tab. I and the ESI text.

An in-depth derivation and explanation of the full quantum theory and all associated parameters are given in a separate manuscript [1]. In Table I we list the parameters that are required to reproduce the simulated diffraction images of Fig. 3 in the main text. The interferometer setup with relevant parameters is also depicted in Fig. 1.

We first find the height of the velocity selection slit y_{02} and the velocity shift $p_{0,z}/m$ for the expansion in the source to reproduce the horizontally integrated signal of the experiment. The height of the light grating $y_{0,g}$ and the optical properties α_r , σ of the molecules are then optimised to find the best agreement with the experimental data. To find the optimum we minimise the residual sum of squares over all pixels of the simulated and experimental image. The experimental data is vertically smoothed for this comparison.

For all cases we assume negligible fluorescence $\phi_F = 0$, perfect reflectivity of the mirror $\eta = 1$ and a vanishing depletion probability. We further assume that internal conversion can be neglected in favour of intersystem crossing

$\phi_{IC} = 0$, $\phi_{ISC} = 1$. The gravitational acceleration is $g = -9.81 \text{ m/s}^2$, the rotation frequency of Earth at Vienna is $\omega \cdot \mathbf{e}_x = 5.4 \times 10^{-5} \text{ s}^{-1}$, and $\omega \cdot \mathbf{e}_y = -4.9 \times 10^{-5} \text{ s}^{-1}$. The screen is discretised in squares of width $d_{\text{px}} = 0.33 \mu\text{m}$, corresponding to the previously calibrated effective size of the pixels recorded by the CCD camera. The images are normalised to unity for the evaluation.

In the case of DND the outlined optimisation procedure is impeded by a vertical bias of the signal most likely caused by inhomogeneous illumination of the diffraction image and the fact that no suitable background data is available. Here we manually set the required parameters to qualitatively reproduce the features of the experimentally observed diffraction image.

Bounds on accuracy and precision

The optimisation procedure described above allows us to reproduce our experimental data and to assign the dominant diffraction processes. In Fig. 2 we show a scan of the possible deep ultraviolet molecular polarizabilities and absorption cross sections, $\alpha_r - \sigma$, that fit the experiment. The heat map shows the natural logarithm of the residual sum of squares computed for the simulation and experimental data. The agreement between experiment and theory allows to estimate an order of magnitude for the DUV polarisabilities and cross sections. Note that the diffraction patterns are insensitive to the sign of the polarizability in this setup. Complementary measurements shall be realised in a revised setup to extract these optical properties with improved accuracy and precision.

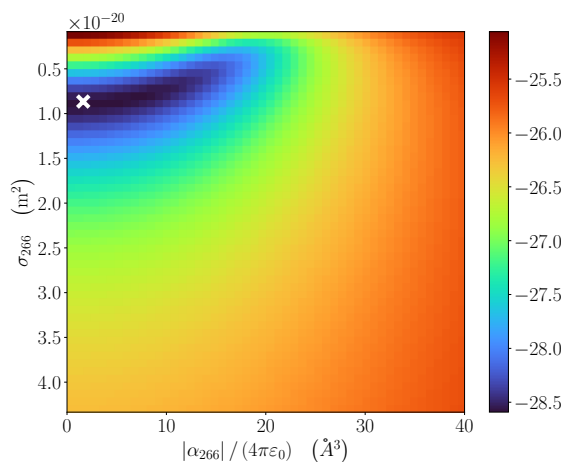


FIG. 2. Natural logarithm of the residual sum of squares as a function of the parameters $|\alpha_{266}|$ and σ_{266} computed for the simulated and experimental data of PcH_2 . Lower values indicate a better agreement between the two datasets. The minimum is marked by a white cross.

SYNTHESIS AND CHARACTERISATION OF ZnPc-NBE_4

General Procedures: All commercially available chemicals were used without further purification. Dry solvents were used as crown cap and purchased from ACROS ORGANICS and SIGMA-ALDRICH. NMR solvents were obtained from CAMBRIDGE ISOTOPE LABORATORIES, INC. (Andover, MA, USA) or SIGMA-ALDRICH. All NMR experiments were performed on BRUKER AVANCE III or III HD, two- or four-channel NMR spectrometers operating at 400.13, 500.13 or 600.27 MHz proton frequency. The instruments were equipped with direct observe BBFO, indirect BBI or cryogenic four-channel QCI (H/C/N/F) 5 mm probes, all with self-shielded z-gradient. The experiments were performed at 298 K or 295 K. All chemical shifts (δ) are reported in parts per million (ppm) relative to the used solvent and coupling constants (J) are given in Hertz (Hz). The multiplicities are written as: s = singlet, d = doublet, t = triplet, dd = doublet of doublet, m = multiplet. Flash column chromatography (FCC) was performed with SiliaFlash® P60 from SILICYCLE with a particle size of 40–63 μm (230-400 mesh), and for TLC silica gel 60 F254 glass plates with a thickness of 0.25 mm from MERCK were used. The detection was carried out with a UV-lamp at 254 or 366 nm. UV/VIS absorption spectra were recorded on a JASCO V-770 Spectrophotometer with a 1 cm quartz glass cuvette. High-resolution mass spectra (HRMS) were measured with a BRUKER MAXIS 4G ESI-TOF instrument or a BRUKER SOLARIX spectrometer with a MALDI source.

Synthetic steps to the target structure: As displayed in Scheme 1, the target structure ZnPc-NBE_4 was assembled in two synthetic steps, followed by purification via sublimation. As the first step, the condensation between (2-nitrophenyl)methanol and 4-hydroxyphthalonitrile provided the phthalonitrile precursor (4-((2-nitrobenzyl)oxy)phthalonitrile) exposing the photocleavable nitro benzyl ether subunit. Its subsequent cyclotramerization in the presence of zinc acetate provided the target structure as mixture of regioisomers. To our delight, sublimation of the crude mixture provided the highly symmetric regioisomer ZnPc-NBE_4 which was used in the experiments reported here.

Synthesis of 4-((2-nitrobenzyl)oxy)phthalonitrile: An oven dried 100 mL round-bottomed flask under argon was charged with (2-nitrophenyl)methanol (1831 mg, 11.6 mmol, 1.0 eq.), 4-hydroxyphthalonitrile (2006 mg, 13.9 mmol, 1.2 eq.), triphenylphosphine (4564 mg, 17.4 mmol, 1.5 eq.) and dry tetrahydrofuran (THF, 50 mL). The reaction mixture was cooled to 0 °C and diisopropyl azodicarboxylate (DIAD, 3.43 mL, 17.4 mmol, 1.5 eq.) was added drop wise. The reaction was allowed to warm up to room temperature and stirred for 12 hours. After TLC confirmed full conversion of the starting materials the solvent was removed under reduced pressure and the remaining residue was purified by column chromatography (ethyl acetate/cyclohexane = 1/2) to yield the desired product as an off-white solid (2000 mg, 11.6 mmol,

Parameter	TPP	PcH ₂	DND
Laser power P_L	0.92 W	0.96 W	1.0 W
Laser waist w_y	13 μm	16 μm	20 μm
Molecule mass m	614.74 u	514.5 u	290.3 u
DUV polarisability $ \alpha_{266} $	$24 \text{ \AA}^3 \cdot 4\pi\epsilon_0$	$1.2 \text{ \AA}^3 \cdot 4\pi\epsilon_0$	$35 \text{ \AA}^3 \cdot 4\pi\epsilon_0$
DUV absorption cross section σ_{266}	$3.4 \times 10^{-21} \text{ m}^2$	$8.5 \times 10^{-21} \text{ m}^2$	$1 \times 10^{-21} \text{ m}^2$
Grating height y_{0g}	-12.7 μm	-5.1 μm	-43.0 μm
Slit height y_{02}	-21.6 μm	-16.5 μm	-54.7 μm
Source temperature T	688 K	746 K	539 K
Slit width x_{c1}	3.5 μm	2.7 μm	5.0 μm
Slit width x_{c2}	1.7 μm	0.6 μm	3.0 μm
Momentum shift $p_{0,z}/m$	117 m s^{-1}	76.5 m s^{-1}	10.2 m s^{-1}
Source size d_s		200 μm	
Slit position y_{01}		0 μm	
Slit width y_{c1}		1 m	
Slit width y_{c2}		20 μm	
Distance L_1		0.52 m	
Distance L_2		0.3 m	
Distance L'_2		0.02 m	
Distance L_3		0.08 m	
Distance L_4		0.69 m	
Distance L'_4		0.605 m	
Grating period d		133 nm	

TABLE I. Parameters used to simulate the diffraction images shows in Fig. 3 of the main text.

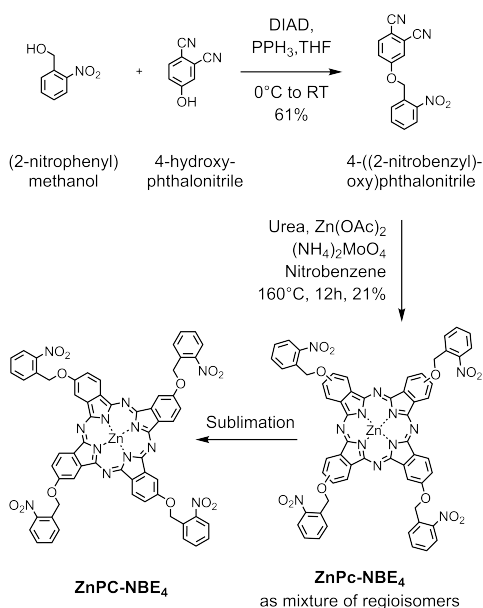
61 %).

Analytical data for 4-((2-nitrobenzyl)oxy) phthalonitrile: ¹H NMR (400 MHz, DMSO-d₆, 22 °C) δ = 8.18 (dd, J = 8.2, 1.3 Hz, 1H), 8.08 (d, J = 8.8 Hz, 1H), 7.91 (d, J = 2.7 Hz, 1H), 7.81 (td, J = 7.6, 1.3 Hz, 1H), 7.74 (dd, J = 7.8, 1.5 Hz, 1H), 7.66 (ddd, J = 8.7, 7.4, 1.5 Hz, 1H), 7.57 (dd, J = 8.9, 2.6 Hz, 1H), 5.66 (s, 2H). ¹³C NMR (101 MHz, DMSO-d₆, 22 °C) δ = 161.18, 147.41, 135.92, 134.25, 131.07, 129.57, 129.21, 125.08, 120.60, 120.44, 116.37, 116.10, 115.63, 106.69, 67.51 ppm. HRMS (ESI-ToF, MeOH, positive mode): calc. for [C₆₀H₃₆N₁₂O₁₂Zn]⁺ 302.0536; found 302.0537.

Synthesis of ZnPc-NBE₄: An oven dried 50 mL round-bottomed flask under argon was charged with 4-((2-nitrobenzyl)oxy)phthalonitrile (2000 mg, 7.16 mmol, 1.0 eq.), urea (1247 mg, 20.8 mmol, 2.9 eq.), zinc acetate (328 mg, 1.79 mmol, 0.28 eq.), ammonium molybdate (28 mg, 0.14 mmol, 0.02 eq.) and were heated in nitrobenzene (30 mL) at 160 °C for 12 h. After cooling, the reaction mixture was treated with water and the green dark product that precipitated was filtered off, successively washed with water, ethyl acetate and ethanol. After evaporation of the solvent under reduced pressure, the crude was purified by column chromatography (acetone/pyridine 5/1 and later 1/1) to obtain the mixture of regioisomers as a blue solid (460 mg, 1.79 mL, 21 %). Sublimation provided the pure regioisomer in yields below 5 %.

Analytical data for ZnPc-NBE₄: ¹H NMR (500 MHz, DMSO-d₆, 22 °C) δ = 9.25 (d, J = 6.8 Hz, 4H), 8.91 (d, J = 20 Hz, 4H), 8.29 (t, J = 7.4 Hz, 4H), 8.19 (d, J = 7.5 Hz, 4H), 7.79 (t, J = 7.6 Hz, 4H), 7.88 (s, 4H), 7.77 (t, J = 7.8 Hz,

4H), 6.05 (s, 8H). HRMS (MALDI, DCM/DCTB Mix 1:10, positive mode): calc. for [C₆₀H₃₆N₁₂O₁₂Zn]⁺ 1180.1862; found 1180.1858.

Scheme 1. Synthesis scheme for the compound ZnPc-NBE₄.

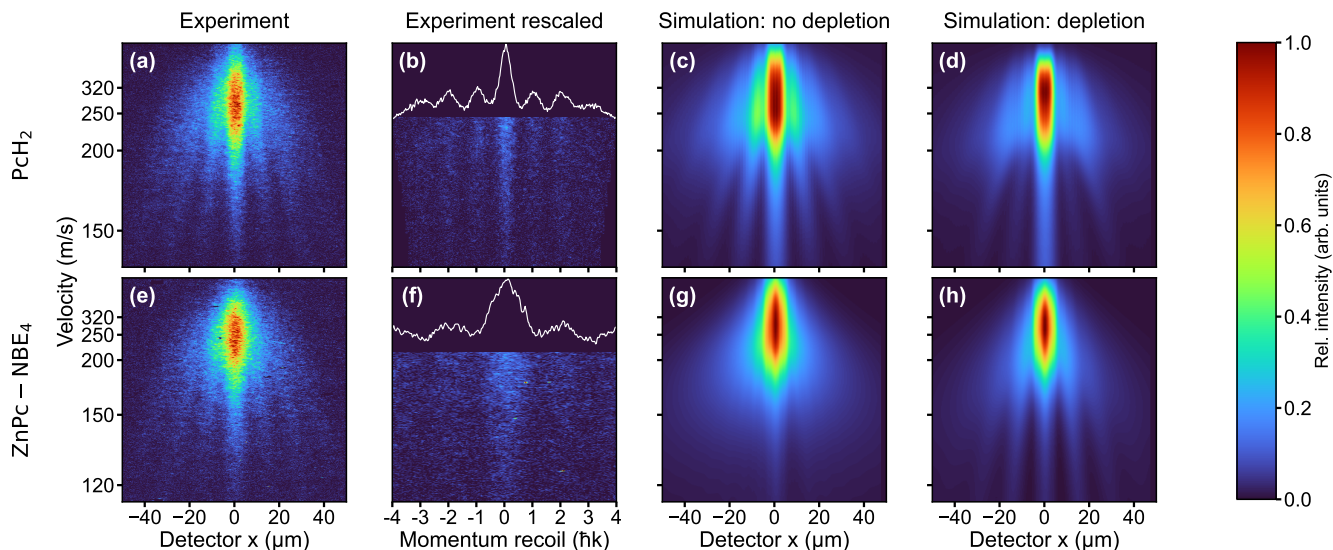


FIG. 3. Comparing the experimental and simulated diffraction patterns of PcH_2 (top row) and ZnPc-NBE_4 (bottom row). The measured patterns ((a), (e)) are nearly identical, suggesting cleavage of ZnPc-NBE_4 . This is further supported by simulation considering effects of depletion for ZnPc-NBE_4 ((g), (h)), where only the latter (assuming the efficient depletion) reproduces the measured data. Note that the opposite is true for PcH_2 .

MEASUREMENTS WITH ZNPC-NBE_4

Interestingly, we find that the the diffraction pattern for ZnPc-NBE_4 is almost identical to that of PcH_2 , as shown in Fig. 3. This invites two complementary interpretations: First, numerical simulations with and without photodissociation of ZnPc-NBE_4 show that the observed fringe pattern can be explained under the assumption that photocleavage is present and efficient (Fig. 3 (g-h)). This is true independent of whether a single, two, three, or all functional groups are split off, if only the intact parent molecules make it to the detector and all fragments are kicked to beyond the detector acceptance angle. The diffraction pattern would look similar to that of PcH_2 because effective cleavage via single photon absorption would remove the absorption fringes. The $n\hbar k$ peaks of PcH_2 (Fig. 3 (a-d)) would therefore be practically co-located with the $2n\hbar k$ peaks of ZnPc-NBE_4 . The second interpretation, however, is also attractive: at a temperature of 400°C all four NBE groups as well as the coordinated Zn atom may already be detached in the thermal source. In this case, the diffraction patterns look identical because the molecules are identical.

To distinguish between these two possibilities one can en-

visage two tests, one based on matter-wave arguments and one using mass spectrometry. Even though the peaks are co-located, the intensity distribution of the interference fringes should depend on the optical polarizability of the arriving molecules - which is substantially bigger for ZnPc-NBE_4 than for PcH_2 . However, since DUV polarisabilities in the gas phase are not available from independent measurements, this interesting route remains closed for now. Re-collecting the emitted molecules on a glass slide behind the oven and post-analysing them in MALDI-MS shows that thermal decomposition is almost complete - encompassing all NBE subgroups down to the bare phthalocyanine core as shown in Fig 4. This underlines the importance of developing non-destructive, bright sources for molecular beams that would allow conducting these and similar experiments with thermally fragile systems.

* ksenija.simonovic@univie.ac.at

† markus.arndt@univie.ac.at

[1] L. Martinetz, B. A. Stickler, K. Simonović, R. Ferstl, C. Brand, M. Arndt and K. Hornberger, *Probing molecular photophysics in a matter-wave interferometer*, 2024, <https://arxiv.org/abs/2407.18775v1>.

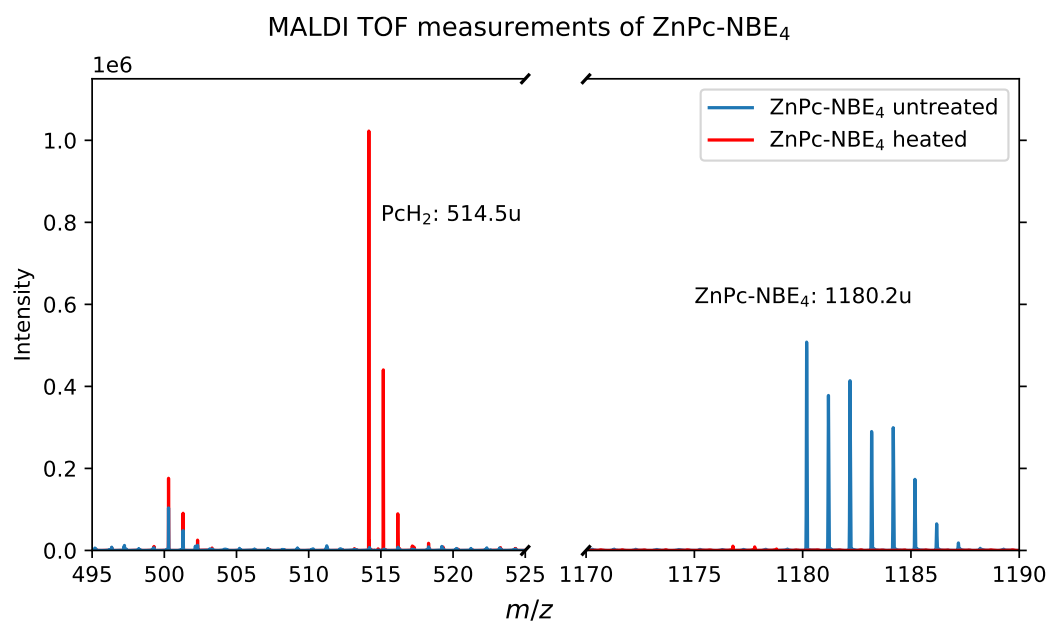


FIG. 4. MALDI-TOF measurements of untreated ZnPc-NBE₄ (blue) and after oven sublimation at temperatures needed to create a molecular beam. While the untreated sample shows a strong peak around 1180 u as expected, the heated one only shows a peak at 514.5 u. This is the mass of the metal-free phthalocyanine core, indicating that the sample undergoes nearly complete thermal decomposition in the source already.